論文 / 著書情報
Article / Book Information

Title	Active-Bending Six-Bar Tensegrity Modular Robot Driven by Thin Artificial Muscles
Authors	Ryota Kobayashi, Hiroyuki Nabae, Koichi Suzumori
Citation	IEEE Robotics and Automation Letters, Volume 8, Issue 11, Page 7400 - 7407
Pub. date	2023, 9
Copyright	(c) 2023 IEEE. Personal use of this material is permitted. Permission from IEEE must be obtained for all other uses, in any current or future media, including reprinting/republishing this material for advertising or promotional purposes, creating new collective works, for resale or redistribution to servers or lists, or reuse of any copyrighted component of this work in other works.
DOI	https://dx.doi.org/10.1109/LRA.2023.3315537
Note	This file is author (final) version.

Active-Bending Six-Bar Tensegrity Modular Robot Driven by Thin Artificial Muscles

Ryota Kobayashi[1], Hiroyuki Nabae[1], and Koichi Suzumori[1]

***Abstract*—Significant progress has been achieved in the development of tensegrity robots with rolling capabilities. However, because rolling robots operate passively due to gravity, they are limited to certain environments. So, our aim is to enhance the versatility of tensegrity robots by modularizing a six-bar tensegrity structure, enabling the robot to operate in more diverse environments. Thus far, we have developed an active and large stretch module and a torsion module with six-bar tensegrity. In this study, we present the design and development of an active and large-bend module for a six-bar tensegrity robot using thin McKibben muscles. Similar to the stretch module developed previously, we employed the 4/3 muscle winding method to create the bend module. This approach enabled approximately 45 deg bending in six different directions. The arrangement of artificial muscles within the bend module is identical to that in the stretch module, allowing not only bending but also stretching and contracting. Further, we successfully constructed a tensegrity arm with bending functionality to demonstrate the capabilities of the bend module. We also conducted a pick-and-place demonstration using the arm to demonstrate the potential application of the bend module.**

***Index Terms*—Tensegrity, bending, thin McKibben muscle, soft robot applications**

I. Introduction

In recent years, many researchers have focused on the flexibility and resilience of tensegrity structures and applied tensegrity structures to robots [1]. Tensegrity robots are more flexible and adaptable to their surrounding environments than conventional rigid robots. Their structural design combining rigid struts and flexible threads enhances their resilience, setting them apart from other soft robots [2] comprising solely of soft bodies and actuators [3][4]. These unique properties are expected to make tensegrity robots useful in unknown spaces such as outer spaces and caves, where flexibility to adapt to the environment and resilience against obstacles are important requirements [5][6].

Tensegrity robots using six bars have been extensively studied [5][7]. The six-bar tensegrity has the simplest configuration of all spherical tensegrity, and this has enabled tensegrity robots to perform the rolling operation [5][8][9]. However, because rolling robots operate passively due to gravity, they are limited to certain environments. Although robots can now climb inclines [10], it is difficult for rolling robots to move in complex and intricate environments such as caves. A tensegrity robot operating in a space such as a cave must perform active movements. However, only few studies have focused on tensegrity robots that perform active movements in a cave-like space, and design methods for such robots are lacking.

Therefore, our aim is to establish a versatile design method for tensegrity robots to develop a six-bar tensegrity robot that can perform contraction, torsion, and bending [6][11]. Furthermore, employing a recurrent neural network (RNN), we aim to realize shape recognition of the surrounding environment by estimating the shape of the tensegrity robot [12]. We presented a module that produces large stretches and contractions [6] and another one that produces large torsions [11] using six-bar tensegrity and thin McKibben muscles [13]. Each module is realized by attaching 12 additional artificial muscles to the six-bar tensegrity structure. An inchworm robot that adapts to its surrounding environment using several stretch modules and a tensegrity robot arm that moves torsionally using torsion modules were also developed. Unlike conventional rolling tensegrity robots, these developed robots are based on active motion and can operate in a wide range of environments. In addition to the stretch and torsion modules, a bend module is also developed to enable the easy design of a tensegrity robot based on the application in this study.

Thus far, several studies have developed tensegrity robots that perform bending deformations [14][15][16][17]. However, many bending deformations are passive deformations caused by external forces [14][15][16] or are small bending deformations in a long series of tensegrities [16][17]. To the best of the authors' knowledge, there is no research on active large bending deformation in the six-bar tensegrity considered in this study. A modular robot, which aims to actively operate in a complex environment, is necessary to realize an active large bending deformation.

This paper describes the bend module developed by extending the stretch module. The configuration of the bend module mirrors that of the stretch module, comprising a six-bar tensegrity framework and an arrangement of 12 thin McKibben muscles based on the 4/3 muscle winding method [6]. By activating different combinations of actuators, the stretch module can also function as a bend module. The utilization of lightweight thin McKibben muscles enables the development of robots that are significantly lighter than those reliant on motors or pneumatic cylinders. Furthermore, the pliable nature of the actuators enables the robot to exploit the

Manuscript received: JUNE, 8, 2023; Revised AUGUST, 16, 2023; Accepted SEPTEMBER, 7, 2023.

This paper was recommended for publication by Editor Yong-Lae Park upon evaluation of the Associate Editor and Reviewers' comments. This work was supported by JSPS International Joint Research Program (JRPs). Number: JPJSJRP20221502.

[1]Ryota Kobayashi, Hiroyuki Nabae, and Koichi Suzumori are with the Department of Mechanical Engineering, Tokyo Institute of Technology, 2-12-1 Ookayama, Meguro-ku, Tokyo 152-8550, Japan kobayashi.r.at@m.titech.ac.jp

Digital Object Identifier (DOI): see top of this page.

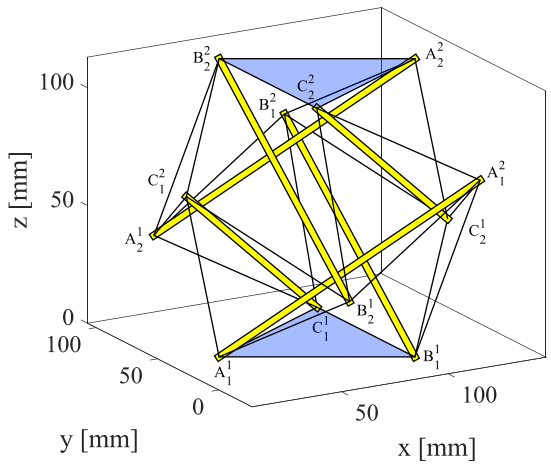

Fig. 1. Six-bar tensegrity used in this study with names and set variables for vertices. The bend of six-bar tensegrity indicates that a tilt exists between the two blue planes.

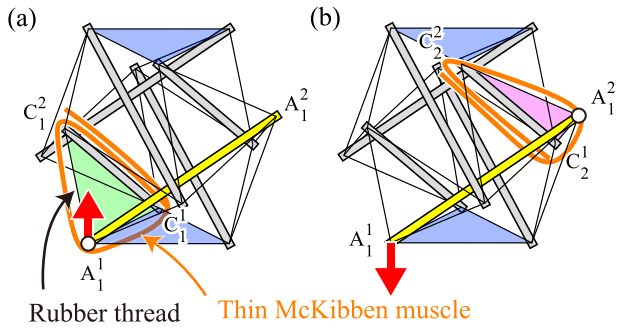

Fig. 2. Two artificial muscles that affect the height displacement of A_1^1 when using the 4/3 muscle winding method. To provide an upward displacement to A_1^1, the artificial muscle in (a) should be driven, and for a downward displacement, the artificial muscle in (b) should be driven.

inherent flexibility of tensegrity structures.

The contribution of this work is establishing the design method of a bend module for a soft tensegrity robot using thin McKibben muscles. Additionally, a tensegrity arm with bending manipulation was constructed to demonstrate the capabilities of the bend module.

The remainder of this paper is organized as follows: Section II describes the concept of bending deformation and the design of the bend module; Section III describes the tensegrity arm created as an application using the bend module; and Section IV presents the conclusions and future plans.

II. Design of Bending Six-bar Tensegrity

A. Concept for bend module

The bending deformation of the six-bar tensegrity is defined as the tilt between $A_1^1B_1^1C_1^1$ and $A_2^2B_2^2C_2^2$, as illustrated in Fig. 1. The six-bar tensegrity is a structure that is symmetrical in three directions. Therefore, if bending deformation can be produced in one direction with artificial muscles placed symmetrically, bending deformation can be achieved in at least three directions. However, artificial muscles cannot be stretched when external forces are applied [18][19]. Therefore, artificial muscles placed to achieve bending in one direction can induce length constraints on bending deformations in other directions, inhibiting deformation. Therefore, this interference needs to be prevented to ensure that bending can be achieved in multiple directions in one module. Thus, considering both the symmetrical arrangement of the artificial muscles to the structure and the interference of the artificial muscles are important when designing a bend module. Therefore, in this study, a bend module is developed by extending a stretch module designed considering the interference caused by the length of the artificial muscles [6].

The stretch module uses a new method of artificial muscle arrangement called 4/3 muscle winding [6]. This method is based on the idea of winding an artificial muscle around an isosceles triangle $\left(\text{e.g. } A_1^1C_1^1C_1^2(\text{Fig. 2(a)})\right)$ that consists of the endpoint of one strut $\left(A_1^1\right)$, another strut $\left(C_1^1C_1^2\right)$, and two rubber threads $\left(A_1^1C_1^1,\ A_1^1C_1^2\right)$ within a six-bar tensegrity, which collapse when the artificial muscle is driven; the strut is made to contact with the endpoint of the strut. In Figs. 2 and 3, the vertices of the isosceles triangle around which the artificial muscle to be driven is wound are indicated by round marks. Stretching and contraction deformations can be achieved by combining this triangular collapsing motion [6]. The six-bar tensegrity consists of six struts and 12 strut endpoints, with each endpoint having an isosceles triangle where the 4/3 muscle winding method can be applied. Therefore, the stretch module contained 12 artificial muscles surrounding each of the 12 triangles. It was described in [6] that contraction deformation can be achieved by driving 6 of the 12 artificial muscles, and extension deformation can be achieved by driving the other 6 artificial muscles. In this study, bending deformation was achieved by changing the combination of the 12 artificial muscles.

A_1^1 was used as an example to consider the effect of a single artificial muscle on the height displacement of the strut endpoints. The two artificial muscles that significantly affected the displacement in the height direction of A_1^1 are shown in Fig. 2(a, b). The two artificial muscles are arranged to surround $A_1^1C_1^1C_1^2$ and $A_1^2C_2^2C_2^1$, respectively. As shown in Fig. 2(a), when the artificial muscle contracts, A_1^1 receives a pull in the direction toward $C_1^1C_1^2$; thus, A_1^1 receives an upward force. The artificial muscle shown in Fig. 2(b) is contracted, A_1^2 receives a pull in the direction of $C_2^2C_2^1$. Meanwhile, strut $A_1^1A_1^2$ is subjected to a downward force, and A_1^1 receives a downward force. Therefore, to displace A_1^1 upward, the artificial muscle in Fig. 2(a) should be driven, and to displace A_1^1 downward, the artificial muscle in Fig. 2(b) should be driven. Thus, the 12 artificial muscles in the structure can be considered artificial muscles that provide upward and downward displacements to the six endpoints of the struts located at the top and bottom of the structure, respectively.

Pneumatic pressure must be applied to the six artificial muscles to displace the endpoints of the top and bottom surfaces for producing a deformation that brings the top and bottom surfaces of the structure closer together, as indicated by

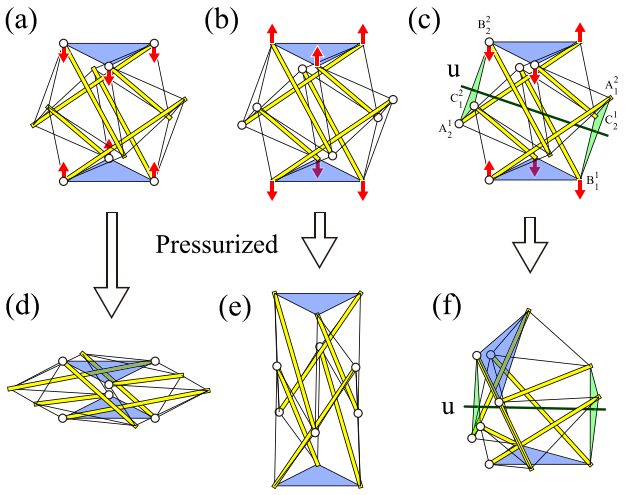

Fig. 3. Artificial muscles to be driven and the deformation at that case. When the artificial muscle is activated to apply the arrow displacement as shown in (a) and (b), the deformations contract as shown in (d) and stretch as shown in (e). The bend deformation (f) can be caused by applying the arrow displacement shown in (c).

the arrows in Fig. 3(a). The deformation illustrated in Fig. 3(d) is the deformation that performs the large axial contraction introduced as Pattern 1 in [6]. Furthermore, when pneumatic pressure is applied to the six artificial muscles to displace each endpoint, as indicated by the arrows in Fig. 3(b), the deformation, as shown in Fig. 3(e), shows the deformation that performs large axial stretching; it is introduced as Pattern 2 in [6].

To generate bending deformation in the structure using 4/3 muscle winding method, pneumatic pressure should be applied to the artificial muscles for displacing each end point as shown by arrows in Fig. 3(c) to provide a tilt between the top and bottom triangles. Bending in other directions can be achieved by rotating or reversing the artificial muscle arrangement shown in Fig. 3(c).

B. Static simulation

As regards the tensegrity analysis, two distinct approaches have been pursued: static analysis [20], which addresses rigidity and stability from a mathematical perspective, and dynamic modeling [21] [22] [23], which handles the dynamic behavior of tensegrity structures subjected to external forces. Recently, the finite element method (FEM) has also been applied for this purpose [24]. In this study, performing a coupled analysis of the force characteristics of the artificial muscle with a conventional tensegrity structural analysis is necessary when considering the force balance of a tensegrity structure integrated with an artificial muscle. Therefore, the authors performed numerical static analyses based on the potential energy in [6] and [11]. In this study, the similar statistical analysis was used.

The arrangement of the six artificial muscles used to produce the displacement as shown in Fig. 3(c) as follows: The vertices of the six isosceles triangles surrounded by the six driven artificial muscles are indicated by round marks in Fig. 3(c), and they are symmetrical about u-axis that passes through the center of gravity of $\mathrm{A}_1^2\mathrm{B}_1^1\mathrm{C}_2^1$ and the center of gravity of $\mathrm{A}_2^1\mathrm{B}_2^2\mathrm{C}_1^2$. Therefore, the six artificial muscles were arranged symmetrically about u-axis. In [11], a method for static simulation of structures when driving artificial muscles symmetrically along one axis is described. This method was applied to simulate the bending deformation.

The rubber thread used for the tensegrity structure in this study is the same as that used in [11]. The rubber threads within the tensegrity structure exhibit slackening upon deformation. To take this into account in the simulation, a functional relationship between the load and length of the rubber was derived, ensuring that the load diminishes to 0 N when the rubber thread shortens below its natural length in [11]. The same values and function were adopted herein for the static simulation. In addition, thin artificial muscles (EM40-1, s-muscle) with force characteristics shown in Fig. 4 are used.

As an example of a simulation of the bending deformation, Fig. 5 shows the analytical results for the deformation of a tensegrity structure whose natural rubber threads length are 50 mm. The endpoints located at the top and bottom of the structure are displaced in the direction indicated by the arrows in Fig. 3(c), and a large bending deformation is observed in the structure as a whole. As with the stretch module [6], artificial muscles are considered to be sagged at 1.1 times the length of the path length to be placed; further, the simulations assume that artificial muscles do not affect the structure when they are sagged. Therefore, the structure did not deform up to approximately 0.18 MPa. In actual tensegrity structures, the positional relationship between the struts changes with the increase in applied air pressure. Upon reaching a specific air pressure threshold, the struts come into contact with one another, effectively curtailing any further deformation of the entire structure. This phenomenon was taken into account during the simulation. A strut diameter D_{strut} and an activated artificial muscle diameter D_{muscle} must be considered owing to the presence of two artificial muscles subjected to pneumatic pressure between $\mathrm{A}_2^1\mathrm{A}_2^2$ and $\mathrm{B}_2^2\mathrm{B}_2^1$ in Fig. 3(c), along with the volume occupied by the strut. The distance between struts $\mathrm{A}_2^1\mathrm{A}_2^2$ and $\mathrm{B}_2^2\mathrm{B}_2^1$ can be expressed as follows:

$$d = \frac{\left|\left(\left(\boldsymbol{A}_2^2 - \boldsymbol{A}_2^1\right) \times \left(\boldsymbol{B}_2^2 - \boldsymbol{B}_2^1\right)\right) \cdot \left(\boldsymbol{B}_2^2 - \boldsymbol{A}_2^2\right)\right|}{\left|\left(\boldsymbol{A}_2^2 - \boldsymbol{A}_2^1\right) \times \left(\boldsymbol{B}_2^2 - \boldsymbol{B}_2^1\right)\right|}. \quad (1)$$

Consequently, the simulation was stopped when the distance between struts $\mathrm{A}_2^1\mathrm{A}_2^2$ and $\mathrm{B}_2^2\mathrm{B}_2^1$ described as d reached the maximum separation $d_{\max}$ given by

$$d_{\max} = D_{\mathrm{strut}} + 2D_{\mathrm{muscle}}. \quad (2)$$

In this case, D_{strut} and D_{muscle} were set at 6 mm and 8 mm, respectively, resulting in a $d_{\max}$ of 22 mm as per Eq. (2). Thus, when the distance d defined by Eq. (1) reached 22 mm, the simulation was terminated and the bending angle of the tensegrity structure at pressures above the pressure causing contact was set to match the bending angle at contact. For example, Fig. 8 shows that during the simulation the struts get in contact under a pressure of approximately 0.24 MPa and a bending angle of 48 deg. Thus, for pressures exceeding 0.24 MPa, the bending angle remained fixed at 48 deg.

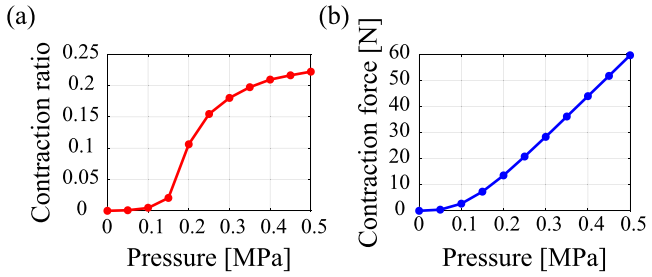

Fig. 4. Force characteristic of thin artificial muscles used in this study.

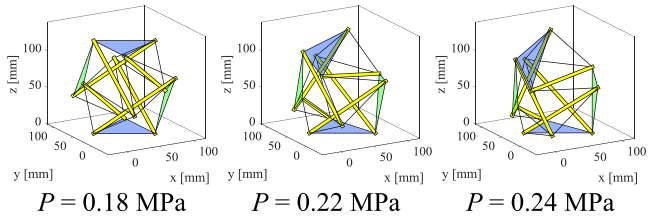

Fig. 5. Simulation result of bending deformation with respect to the pneumatic pressure applied to thin artificial muscles. Artificial muscles are attached in slack conditions and the structure is not deformed up to 0.18 MPa.

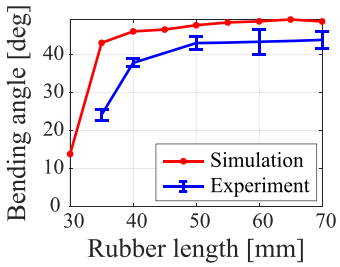

Fig. 6. Bending angle of the bend module with respect to the natural length of the rubber thread when 0.4 MPa is applied to the artificial muscles.

C. Case studies for the bend module design

As shown in [11], the relationship between the generated force and the strain of the rubber thread is highly nonlinear. Therefore, in this study, the natural lengths of the rubber threads are optimized by simulations and experiments using an actual structure; a design method for pre-stretching the rubber thread is described.

The natural lengths of rubber threads comprising the tensegrity were varied, and in each case, the bending deformation was simulated based on Sections II-A and II-B. Furthermore, the bending angle of the tensegrity structure was experimentally confirmed when pneumatic pressure was applied to artificial muscles at 0.4 MPa. Notably, the deformation increased as the pressure raised; hence, although higher pressure levels are desired, pressures above 0.4 MPa tend to cause the breakage of the artificial muscle. As a result, the designated air pressure for utilization is set at 0.4 MPa. It is desirable for the bending angle to be substantial under this specific pressure application to the artificial muscles. Considering this, the pressure was maintained at 0.4 MPa. In this study, the angle of bending deformation Θ of the tensegrity structure is defined by Eq. (3).

$$\Theta = \tan^{-1}\left(\frac{\boldsymbol{a}\cdot\boldsymbol{n}}{|\boldsymbol{a}-(\boldsymbol{a}\cdot\boldsymbol{n})\boldsymbol{n}|}\right), \tag{3}$$

where $\boldsymbol{a}$ represents the vector from the center of gravity of the top triangle to A_2^2, which is displaced upward, and $\boldsymbol{n}$ represents the normal vector of the bottom triangle as defined by the following equation:

$$\begin{aligned}\boldsymbol{a} &= \boldsymbol{A}_2^2 - \frac{1}{3}\left(\boldsymbol{A}_2^2+\boldsymbol{B}_2^2+\boldsymbol{C}_2^2\right),\\ \boldsymbol{n} &= \left(\boldsymbol{B}_1^1-\boldsymbol{A}_1^1\right)\times\left(\boldsymbol{C}_1^1-\boldsymbol{A}_1^1\right).\end{aligned} \tag{4}$$

Equation (3) computes the angle of the slope of $\boldsymbol{a}$ to the bottom triangle $\mathrm{A}_1^1\mathrm{B}_1^1\mathrm{C}_1^1$ using Eq. (4). This is because using the angle between the top and bottom triangles of the tensegrity structure can lead to errors caused by the addition of inclinations in other directions in the actual device. Therefore, Eq. (3) was used in both the simulations and the experiments.

The bending angle of the tensegrity structure when the artificial muscle is driven relative to the natural length of the rubber thread is shown in Fig. 6. To obtain the experimental values, the deformation of the structure is measured five times, and the error bars represent the standard deviation of the measured data. Figure 6 shows that the bending angle of the tensegrity is small when the natural length of the rubber thread is short; the bending angle of tensegrity tends to be constant as the natural length of the rubber thread increases to a certain length. Therefore, in an actual machine, a natural rubber thread length of 50 mm or more would cause sufficient deformation. However, the deformation of the tensegrity structure caused the rubber thread to sag more easily when the natural length of the rubber thread is long. Our goal in environmental shape recognition using tensegrity structures is to estimate the shape of tensegrity structures using the resistance value of a rubber thread, and therefore, it is preferable for the rubber thread not to sag. Therefore, the natural length of the rubber thread was set as 50 mm for this prototype.

The degree of force generated by the rubber threads was considered in the design. In Fig. 6, the bending angle decreases when the natural length of the rubber thread is short. This is because the force generated by the rubber thread is so large that the force of the artificial muscle cannot deform the tensegrity structure. The most elongated rubber thread at $P = 0.24$ MPa in Fig. 5 is 95.8 mm, which is approximately 1.20 times the initial length of 79.6 mm of the rubber thread in the initial condition ($P = 0.00$ MPa). Therefore, in the case of a rubber thread with a natural length of 40 mm, the strain of the most elongated rubber thread is approximately 2.4 times larger, and the generated force is extremely large, as shown in [6]. Therefore, it was experimentally confirmed that the natural length of the rubber thread should be designed such that the force generated by the rubber thread is approximately 5 N, smaller than the force generated by the artificial muscle, while considering that the rubber thread elongates approximately 1.20 times in the simulation. The length of the most elongated rubber thread, shown in Fig. 3(d), is 90.9 mm, and the length of the most elongated rubber thread in Fig. 3(e) is 108 mm, which are 1.14 and 1.37 times the initial state, respectively. These values should be used to determine the natural length

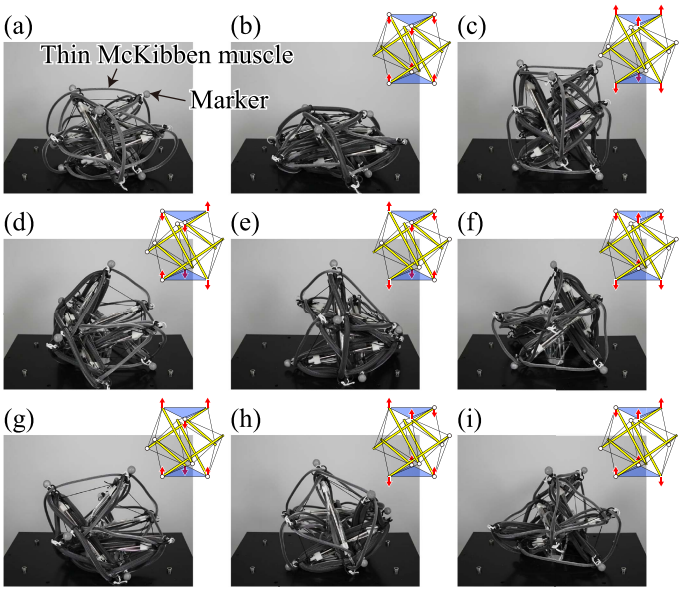

Fig. 7. (a) Initial state of the bend module and (b-i) deformation of the bend module. The method of driving the artificial muscles is shown at the upper right of each picture. (b) Contract deformation. (c) Stretch deformation. (d-i) Bend deformation in six different directions.

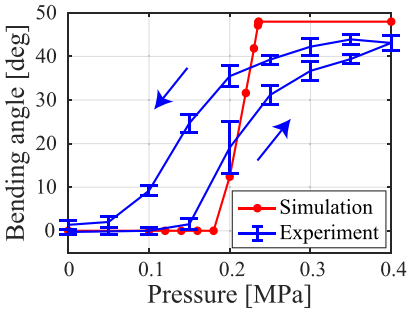

Fig. 8. Bending angle of the bend module with respect to the pneumatic pressure applied to artificial muscles.

of the rubber thread used in the design of the contract, stretch, and bend modules.

The prototype tensegrity structure used to obtain the results in Fig. 6 is shown in Fig. 7(a). In this study, stainless-steel pipes with an outer diameter of 6 mm, inner diameter of 5.4 mm, and length of 130 mm were used as struts of the tensegrity structure. An artificial muscle with force characteristics shown in Fig. 4 is used as the actuator. A version of the components used in [6] with a larger hole was used for the connection between the strut and the rubber thread.

The deformation caused by the artificial muscles of the tensegrity structure with the optimized 50 mm rubber thread is shown in Fig. 7(b-i). The artificial muscle arrangement of the bend module in this study is exactly the same as that of the stretch module [6], and therefore, the contraction and stretching deformations shown in Fig. 7(b) and (c) are possible. Figure 7(d-i) shows the bending deformation of the tensegrity proposed in this study. For each deformation, pneumatic pressure is applied to artificial muscles for displacing the endpoints, as indicated by the arrows in the respective upper-right figures. There are six ways to produce bending deformation, as shown in the upper right diagram of Fig. 7(d-i). These six deformations can be matched by rotating or flipping them, as shown in Fig. 5. Thus, the bending angles of the six deformations are all equal in the simulation.

The change in the bending angle when pneumatic pressure is applied to the artificial muscle of the tensegrity with a natural rubber thread length of 50 mm is shown in Fig. 8. A hysteresis existed between the pneumatic pressure applied to the artificial muscle and the bending angle of the tensegrity in the direction indicated by the arrow in the figure. When the pneumatic pressure of 0.4 MPa was applied, the structure bent approximately 43 deg. However, the differences observed in Figs. 6 and 8 between the experimental and simulated results can be attributed to two primary factors. First, the influence of friction at the bending points of the artificial muscles. As depicted in Fig. 2, the configuration of the artificial muscle can generate high levels of friction during bending, which is not appropriately captured in the simulation, resulting in unaccounted resistance during the experiment. Second, the hysteresis observed in the force response of both the artificial muscles and the rubber threads, as shown in [11] and Fig. 4. The intricate hysteretic load-strain relationship is omitted from the simulation, causing a disparity between the predicted and actual behaviors of the structure.

The bending angles of the bend module developed in this study were compared with those of the tensegrity in other studies. The longer the axial length of the tensegrity ℓ, the greater is the bending angle. The larger the diameter of tensegrity d, the smaller is the bending angle. For this reason, comparisons were conducted using the normalized bending angle, obtained by dividing the bending angle after deformation by ℓ/d of the pre-deformation tensegrity. If the length of the strut is L, the height of a single six-bar tensegrity ℓ is $\sqrt{3}L/2$ and the diameter d is $\sqrt{42}L/6$. Therefore, by dividing 43 deg by ℓ/d, the bending angle normalized by ℓ/d for the bend module in this study is approximately 54 deg. The ℓ/d value of the tensegrity of [16] is approximately 2.4 from Fig. 2E of [16], and the bending angle is approximately 90 deg from Fig. 2H of [16]. Therefore, the bending angle normalized by ℓ/d is approximately 38 deg. The pre-deformation ℓ/d values of the tensegrity of [17] are approximately seven from Fig. 3 of [17], and the maximum bending angle is less than 180 deg from Fig. 11 of [17]. Therefore, the bending angle normalized by ℓ/d is less than 26 deg. Therefore, the bending angle of the bend module developed in this study are 1.4 and 2.1 times larger than the bending angles of the tensegrity structures in the previous studies.

III. Design, Evaluation, and Demonstration of Tensegrity Robotic Arm with the Bend Module

A. Design and development

A bendable tensegrity robotic arm is fabricated by connecting two bend modules, I and II, as shown in Fig. 9(a). The modules are connected to each other so that the two

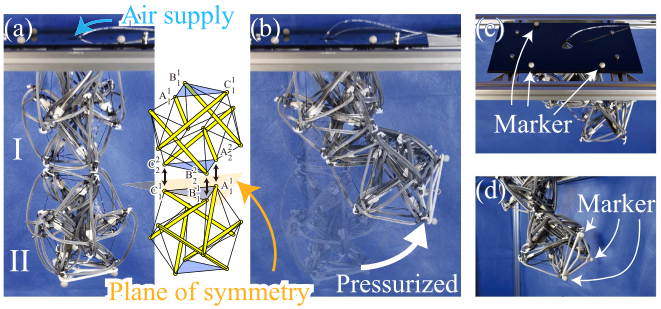

Fig. 9. (a) Developed tensegrity arm consisting of two bend modules. The two structures are connected so that they are mirror images with respect to the plane of symmetry. (b) Bending deformation when 0.4 MPa is applied to the artificial muscles. (c, d) Motion capture markers attached to the tensegrity arm.

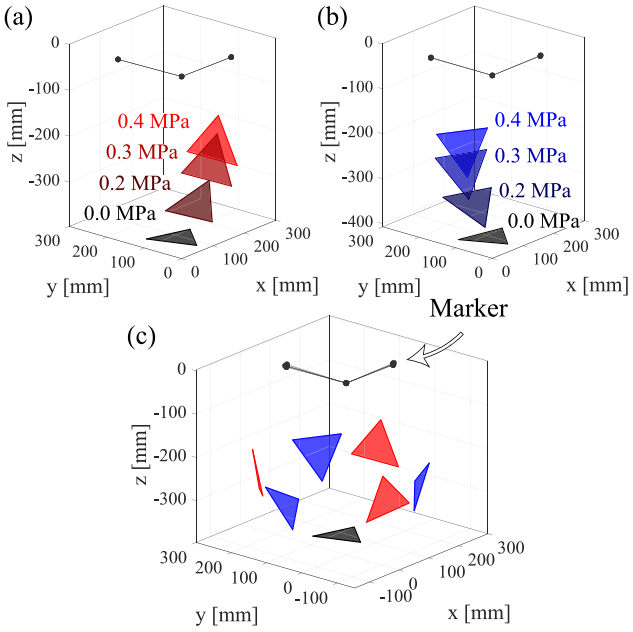

Fig. 10. Trajectory of the arm tip when the pneumatic pressure is varied. There are two patterns shown in (a) and (b). As shown in (c), the arm tip can move in six directions.

modules have a plane-symmetrical relationship. The top and bottom triangles are equilateral triangles in the tensegrity structure with no artificial muscle drive. However, the lengths of the three sides of the top and bottom triangles differ when the pneumatic pressure is applied to the artificial muscle. Therefore, depending on the method used to connect the bend modules, an extra force may be applied to the connection. Therefore, pneumatic pressure is applied to the artificial muscle to deform the two modules such that they are in a mirror image relationship with the boundary of the two modules as the symmetry plane. Modules I A_2^2 and II A_1^1, I B_2^2 and II B_1^1, and I C_2^2 and II C_1^1 are tied together using rubber threads. Each arm weighed 412 g. The root of the arm (i.e., $A_1^1B_1^1C_1^1$ in module I) is fixed to the board, as shown in Fig. 9(a).

Figure 9(d) shows that a triangular component fabricated using a 3D printer is attached to the tip of Module II. A hook is attached to the center of the triangle, from which a weight can be suspended. In addition, three motion capture markers were attached to the board on which the arm was mounted, and three motion capture markers were attached to the tip of the arm, as shown in Fig. 9(c, d). By measuring the positions of these markers, it is possible to measure the position of the arm tip when the tensegrity is deformed, as shown in Fig. 9(b). Figure 9(b) shows conditions of the tensegrity arm when 0.4 MPa is applied to the artificial muscle.

B. Evaluation under no load

There are six methods to drive the 12 artificial muscles for the bending deformation of one module, as shown in Fig. 7(d-i). So, there are also six bending methods for the arm. One deformation that displaces only one of the tip triangles upward is shown in Fig. 10(a), and the one that displaces two of the tip triangles upward is shown in Fig. 10(b). The positions of the motion-capture markers at the tip of the arm shown in Fig. 9(d) are indicated when 0.0 MPa, 0.2 MPa, 0.3 MPa, and 0.4 MPa are applied to the artificial muscles. The pneumatic fitting shown of [6] is used, and pneumatic pressure is supplied to all artificial muscles to be driven by a single pneumatic hose.

The six positions of the arm tip under six different bending deformations are shown in Fig. 10(c). These are the positions of the motion-capture markers at the arm tip when 0.4 MPa is applied, indicating that bending in six directions can be realized. In Fig. 10(c), one of the triangles at the tip with one point displaced upward (Fig. 10(a) pattern) is red, and the two points displaced upward (Fig. 10(b) pattern) are blue.

The magnitudes of the bending angles of the deformations for the patterns shown in Figs. 10(a) and 10(b) are different. The average deformation bending angles in the three directions for each pattern are 83.2 deg for the pattern shown in Fig. 10(a) and 75.8 deg for the pattern shown in Fig. 10(b). The bending angle is defined as the angle between the planes consisting of motion captures of the three points in Fig. 9(c) and the plane consisting of the motion capture of the three points in Fig. 9(d). The bending deformations in a single structure are ideally equal, as shown in Fig. 7(d-i). However, it is possible that triangular restraints at the tips and root of the arm affect the bending deformations.

C. Evaluation with load

Changes in the bending angle of the tensegrity arm were recorded when the weight was hung from the tip of the arm after the arm was bent using an artificial muscle. The artificial muscles are first subjected to a pneumatic pressure of 0.4 MPa, which causes the deformation illustrated in Fig. 10(a). Subsequently, weights of 100 g each are incrementally added up to a total of 600 g. Thereafter, the weights are removed one by one. Throughout this process of adding and removing weights, the corresponding bending angles are measured and recorded. The displacement of the arm bending angle with respect to the moment of force applied to the base of the arm by the weight is shown in Fig. 12. Although the mass of the tensegrity arm is 412 g, the displacement angle is 23 deg (the initial

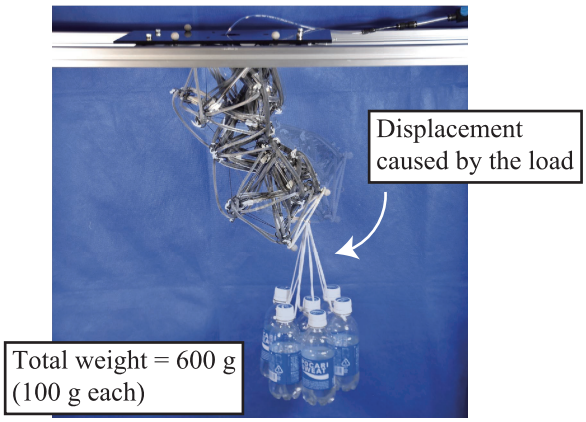

Fig. 11. Deformation when a total weight of 600 g is suspended at the tip of the arm with the arm bent.

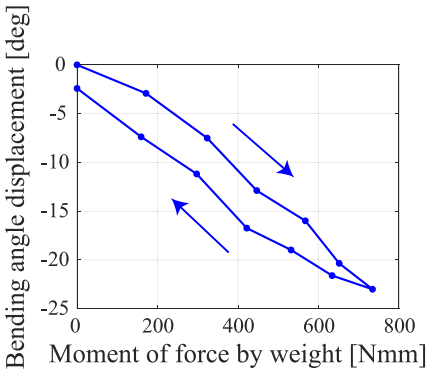

Fig. 12. Bending angle displacement of the arm when a moment is applied to the root of the arm by a weight.

bending angle is 83.2 deg), even when subjected to a moment of 700 Nmm. The bend module can be used to manipulate objects that are 1.5 times heavier than their own weight against gravity.

D. Demonstration

Figure 13(a) shows that the tensegrity grip module described in [11] is attached to the tip of the robot arm. The tensegrity robot arm presented in [11] combines contract module as well as grip and torsion modules. However, the bend module can perform not only bending deformation but also contraction deformation; therefore, it can assume the function of a contract module without a stand-alone contract module. This grip module is approximately 70 g, which is within the range of the load from the weights tested in III-C, and a sufficient bending deformation of the arm is expected, when considering the increased moment of force caused by the shift of the center of gravity of the grip module. Then, a demonstration is presented to pick and place a ball with a diameter of 40 mm and a weight of approximately 2.3 g.

The experimental setup is illustrated in Fig. 13(a), where a rail made of an aluminum frame is placed on the lower side of the arm to line up the balls. The second and subsequent balls rolled downward when the first object is lifted by placing

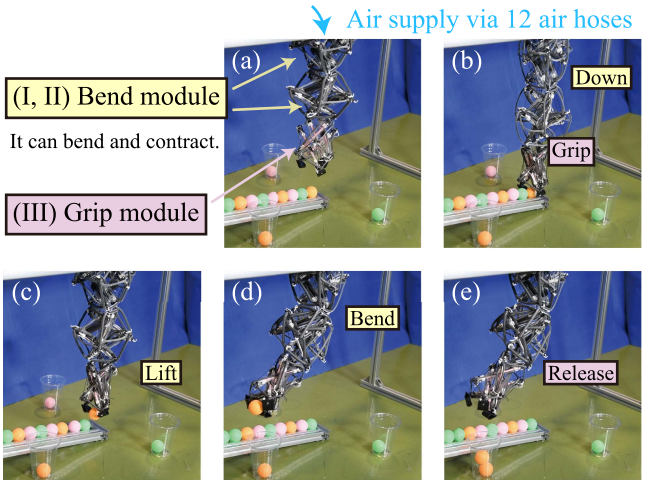

Fig. 13. Demonstration of the tensegrity arm with grip module attached to pick and place the balls. (a) Initial state. (b) Down the arm and grip the ball. (c) Lift the arm. (d) Move and sort balls according to their colors in three directions. (e) Release the ball.

the rails at an angle. This ensures that the object is always present on the underside of the arm and that the object can be continuously picked by the arm. In addition, 13 pneumatic hoses are attached to the arms. Between the two modules, artificial muscles, which are mirror images of each other with respect to the plane of symmetry shown in Fig. 9(a), are connected by pneumatic hoses. 12 pneumatic tubes are attached to apply pneumatic pressure to each pair of artificial muscles. The remaining pneumatic hose is used to drive the grip module. A total of 13 solenoid valves were used to determine which pneumatic hoses would apply the pneumatic pressure.

A demonstration of sorting each of the three colored balls from the rail into cups positioned in the three directions is presented. In the initial state, as shown in Fig. 13(a), bend modules I and II are in a contracted state. First, the arm tip is displaced downward by releasing pneumatic pressure from the artificial muscles of the bend module, as shown in Fig. 13(b). After 0.5 s, the ball is grasped while the grip module is driven. After 0.5 s, the ball is lifted by contracting the bend module, as shown in Fig. 13(c), and after another 0.5 s, the ball is moved to the upper side of the cup by driving the bend module in the direction that matches the color, as shown in Fig. 13(d). 0.5 s later, the ball is released by the grip module and placed in a cup, as shown in Fig. 13(e). Then, after 0.5 s, it returns to the state shown in Fig. 13(a), and 1.0 s after that, it deforms as shown in Fig. 13(b). This enables a continuous pick-and-place operation, and it takes 3.5 s per each ball sorting. However, the arrangement of the tri-color balls is pre-established. Therefore, the robotic arm simply follows a predetermined sequence and no visual closed-loop control is performed. As shown in the supplementary video file, each of the three colored balls can be sorted into cups arranged in three different directions.

IV. Conclusion

This study described the achievement of active and large bending deformations of six-bar tensegrity. The stretch module

developed in [6] was extended to realize an active bending deformation of approximately 45 deg in each of the six directions. The module has 12 attached artificial muscles, and it was shown by changing the combination of the driven artificial muscles; the structure as a whole can perform bending, contraction, and stretching deformations.

A robot arm was fabricated using the bend module, and the deformation was checked when no load was applied and when load was applied. The mass of the tensegrity arm integrated with the thin artificial muscles was as light as 412 g; however, it was shown that the displacement was limited to approximately 20 deg even when a 600 g weight was hung while the arm was bent by approximately 80 deg. Furthermore, a ball pick-and-place operation was performed by attaching a grip module weighing 70 g to the end of the arm, which demonstrated one of the applications of the bend module.

In future, we plan to realize a tensegrity robot that can explore unknown environments by modularizing the "stretch, contract, torsion, and bending" functions that have been realized so far. We plan to recognize the shape of the surrounding environment from the robot's own shape estimation using an RNN as the robot progresses through the environment.

REFERENCES

[1] D. S. Shah, J. W. Booth, R. L. Baines, K. Wang, M. Vespignani, K. Bekris, and R. Kramer-Bottiglio, "Tensegrity robotics," *Soft robotics*, 2021.

[2] G. M. Whitesides, "Soft robotics," *Angewandte Chemie International Edition*, vol. 57, no. 16, pp. 4258–4273, 2018. [Online]. Available: https://onlinelibrary.wiley.com/doi/abs/10.1002/anie.201800907

[3] K. Suzumori, S. Iikura, and H. Tanaka, "Flexible microactuator for miniature robots," in *[1991] Proceedings. IEEE Micro Electro Mechanical Systems*, 1991, pp. 204–209.

[4] Z. Mao, T. Iizuka, and S. Maeda, "Bidirectional electro-hydrodynamic pump with high symmetrical performance and its application to a tube actuator," *Sensors and Actuators A: Physical*, vol. 332, p. 113168, 2021. [Online]. Available: https://www.sciencedirect.com/science/article/pii/S0924424721006312

[5] M. Vespignani, J. M. Friesen, V. SunSpiral, and J. Bruce, "Design of superball v2, a compliant tensegrity robot for absorbing large impacts," in *2018 IEEE/RSJ International Conference on Intelligent Robots and Systems (IROS)*, 2018, pp. 2865–2871.

[6] R. Kobayashi, H. Nabae, G. Endo, and K. Suzumori, "Soft tensegrity robot driven by thin artificial muscles for the exploration of unknown spatial configurations," *IEEE Robotics and Automation Letters*, vol. 7, no. 2, pp. 5349–5356, 2022.

[7] R. Terajima, K. Inoue, S. Yonekura, K. Nakajima, and Y. Kuniyoshi, "Behavioral diversity generated from body–environment interactions in a simulated tensegrity robot," *IEEE Robotics and Automation Letters*, vol. 7, no. 2, pp. 1597–1604, 2022.

[8] R. L. Baines, J. W. Booth, and R. Kramer-Bottiglio, "Rolling soft membrane-driven tensegrity robots," *IEEE Robotics and Automation Letters*, vol. 5, no. 4, pp. 6567–6574, 2020.

[9] Y. Koizumi, M. Shibata, and S. Hirai, "Rolling tensegrity driven by pneumatic soft actuators," in *2012 IEEE International Conference on Robotics and Automation*, 2012, pp. 1988–1993.

[10] L.-H. Chen, B. Cera, E. L. Zhu, R. Edmunds, F. Rice, A. Bronars, E. Tang, S. R. Malekshahi, O. Romero, A. K. Agogino, and A. M. Agogino, "Inclined surface locomotion strategies for spherical tensegrity robots," in *2017 IEEE/RSJ International Conference on Intelligent Robots and Systems (IROS)*, 2017, pp. 4976–4981.

[11] R. Kobayashi, H. Nabae, and K. Suzumori, "Large torsion thin artificial muscles tensegrity structure for twist manipulation," *IEEE Robotics and Automation Letters*, vol. 8, no. 3, pp. 1207–1214, 2023.

[12] W.-Y. Li, A. Takata, H. Nabae, G. Endo, and K. Suzumori, "Shape recognition of a tensegrity with soft sensor threads and artificial muscles using a recurrent neural network," *IEEE Robotics and Automation Letters*, vol. 6, no. 4, pp. 6228–6234, 2021.

[13] S. Wakimoto, K. Suzumori, and J. Takeda, "Flexible artificial muscle by bundle of mckibben fiber actuators," in *2011 IEEE/ASME International Conference on Advanced Intelligent Mechatronics (AIM)*, 2011, pp. 457–462.

[14] S. Lessard, J. Bruce, E. Jung, M. Teodorescu, V. SunSpiral, and A. Agogino, "A lightweight, multi-axis compliant tensegrity joint," in *2016 IEEE International Conference on Robotics and Automation (ICRA)*, 2016, pp. 630–635.

[15] W.-Y. Li, H. Nabae, G. Endo, and K. Suzumori, "New soft robot hand configuration with combined biotensegrity and thin artificial muscle," *IEEE Robotics and Automation Letters*, vol. 5, no. 3, pp. 4345–4351, 2020.

[16] H. Lee, Y. Jang, J. K. Choe, S. Lee, H. Song, J. P. Lee, N. Lone, and J. Kim, "3d-printed programmable tensegrity for soft robotics," *Science Robotics*, vol. 5, no. 45, p. eaay9024, 2020.

[17] S. Ikemoto, K. Tsukamoto, and Y. Yoshimitsu, "Development of a modular tensegrity robot arm capable of continuous bending," *Frontiers in Robotics and AI*, vol. 8, 2021. [Online]. Available: https://www.frontiersin.org/articles/10.3389/frobt.2021.774253

[18] S. Tanaka, H. Nabae, and K. Suzumori, "Back-stretchable mckibben muscles: Expanding the range of antagonistic muscle driven joints," *IEEE Robotics and Automation Letters*, vol. 8, no. 9, pp. 5331–5337, 2023.

[19] G. Na, H. Nabae, and K. Suzumori, "Braided thin mckibben muscles for musculoskeletal robots," *Sensors and Actuators A: Physical*, vol. 357, p. 114381, 2023. [Online]. Available: https://www.sciencedirect.com/science/article/pii/S0924424723002303

[20] S. H. Juan and J. M. M. Tur, "Tensegrity frameworks: Static analysis review," *Mechanism and Machine Theory*, vol. 43, no. 7, pp. 859–881, 2008.

[21] J. M. M. Tur and S. H. Juan, "Tensegrity frameworks: Dynamic analysis review and open problems," *Mechanism and Machine Theory*, vol. 44, no. 1, pp. 1–18, 2009.

[22] H. Murakami, "Static and dynamic analyses of tensegrity structures. part 1. nonlinear equations of motion," *International Journal of Solids and Structures*, vol. 38, no. 20, pp. 3599–3613, 2001.

[23] H. Murakami, "Static and dynamic analyses of tensegrity structures. part ii. quasi-static analysis," *International Journal of Solids and Structures*, vol. 38, no. 20, pp. 3615–3629, 2001.

[24] Z. Kan, H. Peng, B. Chen, and W. Zhong, "Nonlinear dynamic and deployment analysis of clustered tensegrity structures using a positional formulation fem," *Composite Structures*, vol. 187, pp. 241–258, 2018. [Online]. Available: https://www.sciencedirect.com/science/article/pii/S0263822317331975